

Dietary pectic glycans are degraded by coordinated enzyme pathways in human colonic *Bacteroides*

Ana S. Luis¹, Jonathon Briggs¹, Xiaoyang Zhang¹, Benjamin Farnell^{2,3}, Didier Ndeh¹, Aurore Labourel¹, Arnaud Baslé¹, Alan Cartmell¹, Nicolas Terrapon⁴, Katherine Stott⁵, Elisabeth C. Lowe¹, Richard McLean², Kaitlyn Shearer², Julia Schüchel⁶, Immacolata Venditto¹, Marie-Christine Ralet⁷, Bernard Henrissat^{4,8,9}, Eric C. Martens¹⁰, Steven C. Mosimann³, D. Wade Abbott^{2,3*} and Harry J. Gilbert^{1*}

The major nutrients available to human colonic *Bacteroides* species are glycans, exemplified by pectins, a network of covalently linked plant cell wall polysaccharides containing galacturonic acid (GalA). Metabolism of complex carbohydrates by the *Bacteroides* genus is orchestrated by polysaccharide utilization loci (PULs). In *Bacteroides thetaiotaomicron*, a human colonic bacterium, the PULs activated by different pectin domains have been identified; however, the mechanism by which these loci contribute to the degradation of these GalA-containing polysaccharides is poorly understood. Here we show that each PUL orchestrates the metabolism of specific pectin molecules, recruiting enzymes from two previously unknown glycoside hydrolase families. The apparatus that depolymerizes the backbone of rhamnogalacturonan-I is particularly complex. This system contains several glycoside hydrolases that trim the remnants of other pectin domains attached to rhamnogalacturonan-I, and nine enzymes that contribute to the degradation of the backbone that makes up a rhamnose-GalA repeating unit. The catalytic properties of the pectin-degrading enzymes are optimized to protect the glycan cues that activate the specific PULs ensuring a continuous supply of inducing molecules throughout growth. The contribution of *Bacteroides* spp. to metabolism of the pectic network is illustrated by cross-feeding between organisms.

The human gut microbiota (HGM)¹ impacts on host physiology and health^{2,3}. Understanding the mechanisms of nutrient acquisition by the HGM, exemplified by glycan metabolism⁴⁻⁶, underpins the development of probiotic and prebiotic strategies that maximize human health. Glycan acquisition by human colonic *Bacteroides* species is well established⁷⁻¹⁰, but it should be emphasized that Firmicutes are more abundant in the HGM of Western populations; however, the mechanism by which they metabolize complex carbohydrates is less well understood⁴. Indeed, it is likely to be that Firmicutes make a substantial contribution to the degradation of dietary and host glycans in the HGM. The glycan-degrading systems of Bacteroidetes are encoded by PULs that are activated by the target carbohydrate⁴. These systems comprise surface glycan binding proteins (SGBPs), outer membrane oligosaccharide transporters; SusC and SusD homologues (SusC_H and SusD_H, respectively), and surface and periplasmic carbohydrate active enzymes (CAZymes) that are grouped into sequence-based families in the CAZy database¹¹. Relevant to this work are glycoside hydrolase (GH) and polysaccharide lyase (PL) families¹².

Pectins are D-galacturonic acid (D-GalA)-rich plant cell wall polysaccharides that are abundant in fruits and vegetables. The two major pectins (see ref. ¹ for review) are homogalacturonan (HG) and rhamnogalacturonan-I (RGI) (Fig. 1a). HG comprises α -1,4-linked D-GalA and the backbone of RGI is a repeating unit of the disaccharide α -1,2-L-rhamnose (Rha)- α -1,4-D-GalA. Depending on the plant species, the RGI backbone is decorated with galactans (β -1,4-D-galactose (D-Gal) units) and/or arabinans (α -1,5-linked L-arabinofuranose (L-Araf) units with additional L-Araf side-chains)¹³. The backbones of HG and RGI are covalently linked¹⁴. Although individual microbial pectin-degrading enzymes have been described¹⁵, the mechanism by which these biocatalysts participate in the concerted degradation of intact pectin remains opaque. *Bacteroides thetaiotaomicron*, a member of the HGM, utilizes all known pectins structures and discrete PULs activated by these glycans have been identified¹⁶. Here we have characterized the function of PULs associated with pectin metabolism and explored how they contribute to interactions within the HGM foodweb. The data show how these loci coordinate the complex degradative

¹Institute for Cell and Molecular Biosciences, Newcastle University, Newcastle upon Tyne, UK. ²Lethbridge Research and Development Centre, Agriculture and Agri-Food Canada, Lethbridge, Alberta, Canada. ³Department of Chemistry and Biochemistry, University of Lethbridge, Lethbridge, Alberta, Canada.

⁴Architecture et Fonction des Macromolécules Biologiques, Centre National de la Recherche Scientifique (CNRS), Aix-Marseille University, Marseille, France. ⁵Department of Biochemistry, University of Cambridge, Cambridge, UK. ⁶Department of Plant and Environmental Sciences, Faculty of Science, University of Copenhagen, Copenhagen, Denmark. ⁷INRA, UR1268 Biopolymères Interactions Assemblages, Nantes, France. ⁸INRA, USC 1408 AFMB, Marseille, France. ⁹Department of Biological Sciences, King Abdulaziz University, Jeddah, Saudi Arabia. ¹⁰Department of Microbiology and Immunology, University of Michigan Medical School, Ann Arbor, MI, USA. Ana S. Luis, Jonathon Briggs and Xiaoyang Zhang contributed equally to this work.

*e-mail: wade.abbott@agr.gc.ca; harry.gilbert@ncl.ac.uk

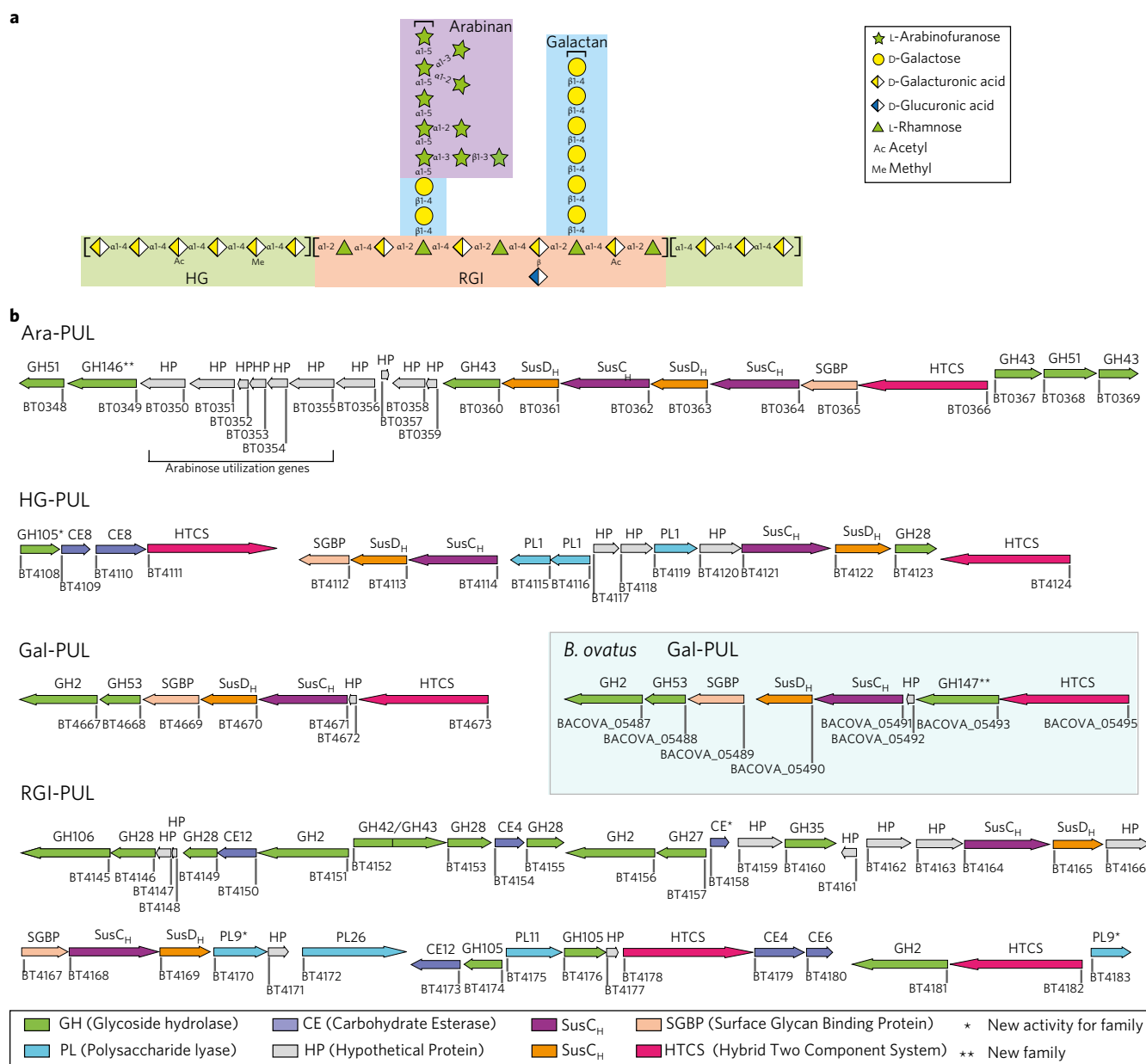


Fig. 1 | Genomic organization of pectin PULs. **a**, Schematic of pectin structure showing the different polysaccharides highlighted with different coloured backgrounds. The respective linkages and monosaccharide composition are represented according to the Symbol Nomenclature for Glycans system⁵⁰. **b**, Genes encoding proteins of known or predicted functionalities are colour coded. GHs, CEs and PLs located in a known CAZyme family are indicated by GHXX, CEXX or PLXX, where XX indicates the number of the family.

interactions between the backbone and oligosaccharide decorations of these acidic polysaccharides.

Results

The PULs that orchestrate pectin degradation were identified from transcriptomic data¹⁶. PULs upregulated in response to arabinan (*bt0348-bt0369*, Ara-PUL), galactan (*bt4667-bt4673*, Gal-PUL), RGI backbone (*bt4145-bt4183*, RGI-PUL) and HG (*bt4108-bt4124*, HG-PUL) were identified (Fig. 1b). To determine the mechanisms by which these loci mediate pectin degradation, the biochemical functions of recombinant proteins encoded by the PULs were determined (Supplementary Tables 1–5).

Initial degradation of the pectins by *B. thetaiotaomicron* is mediated by endo-acting CAZymes on the surface of the bacterium (Fig. 2c and Supplementary Fig. 1). These enzymes are essential

for pectin utilization as they generate glycans with an appropriate degree of polymerization (DP) for transport into the periplasm¹⁷. Consistent with this premise, deletion of the genes encoding the single outer membrane endo-acting enzymes encoded by RGI-PUL (BT4170) and Gal-PUL (BT4668) (Supplementary Fig. 2 and Fig. 2c) prevented growth on the respective pectin (Fig. 2a). The surface location of these enzymes was consistent with whole cell assays of *B. thetaiotaomicron* under aerobic conditions (Fig. 2b), which report only the activity of surface proteins. To explore the function of the rhamnagalacturonan lyase BT4170, a key component of the RGI-degrading apparatus, the crystal structure of the enzyme was determined in complex with ligands. The data (Supplementary Fig. 3) showed that the catalytic apparatus of BT4170 and a HG lyase (Pel9A, 1RU4), both located in family PL9, comprising a Brønsted base (Lys285 in BT4170) and a calcium,

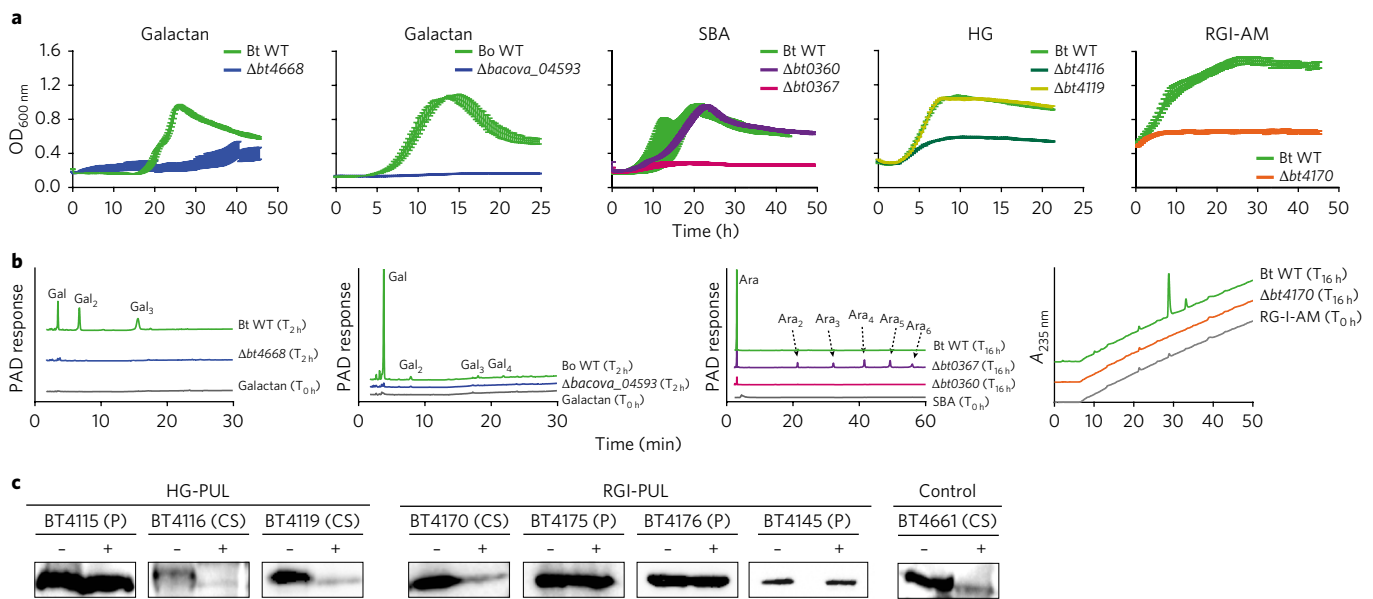


Fig. 2 | Depolymerization of pectins at the cell surface of *B. thetaiotaomicron* cell surface. a, Growth of wild-type and mutants of *B. thetaiotaomicron* (Bt WT and $\Delta btxxxx$) or *B. ovatus* (Bo WT and $\Delta bacova_xxxx$) in minimal media containing the indicated pectic polysaccharide. SBA, sugar beet arabinan; RGI-AM, rhamnogalacturonan I backbone from *Arabidopsis* mucilage (biological replicates, $n=3$, error bars denote the s.e.m.). **b**, Bt WT, Bo WT and mutants lacking functional outer membrane enzymes were incubated with appropriate polysaccharides in aerobic conditions for the times indicated (T_{xh}). Under these conditions substrate is only available to the surface enzymes. Products released from the glycans were monitored by HPAEC with pulsed amperometric detection (PAD) or ultraviolet detection at 235 nm (A_{235nm}). The degree of polymerization of peaks corresponding to the galactose (Gal.) and arabinose (Ara.) oligosaccharides are shown in subscript numbers. **c**, Western blot detection of selected *B. thetaiotaomicron* enzymes encoded by HG-PUL and RGI-PUL after treatment with proteinase K (+) or untreated (-). BT4661 is a known surface glycan binding protein (control)⁷. The cellular localization is indicated as periplasmic (P) or cell surface (CS). The example is from biological replicates $n=3$. The full western blots are shown in Supplementary Fig. 1.

was conserved. Specificity determinants were identified in subsites distal to the active site, explaining why Pel9A and BT4170 target distinct substrates (see Supplementary Information and Supplementary Fig. 3).

Ara-PUL and HG-PUL each encode two surface enzymes. The enzymes derived from Ara-PUL, BT0360 and BT0367, are α -1,5-arabinanases that display endo- and endo-processive activity, respectively (Supplementary Fig. 4 and Supplementary Information). Only $\Delta bt0367$ led to the loss of the arabinan utilization phenotype (Fig. 2a). Gene deletion studies showed that of the two surface PLs (BT4116 and BT4119, Supplementary Fig. 4 and Supplementary Table 2) encoded by HG-PUL, only BT4116 was essential for growth on HG (Fig. 2a). The functional significance of BT0360 and BT4119 is unclear, but may reflect the targeting of substrates not evaluated here.

Gene deletion studies explored the functional significance of the SusC_H-SusD_H pairs encoded by each pectin PUL (Supplementary Fig. 5). In HG-PUL, which contains two SusC_H-SusD_H pairs, only the $\Delta bt4114$ mutant displayed no growth on HG, indicating that BT4114 plays a key role in the import of this pectic glycan. Similarly, the Ara-PUL encodes two pairs of SusC_H-SusD_H transporters (BT0361-BT0362 and BT0363-BT0364)¹⁶. Deletion of *bt0364*, but not *bt0362*, prevented growth on arabinan. This indicates that only the BT0363-BT0364 complex is capable of transporting arabinooligosaccharide products. The rationale for the presence of two SusC_H-SusD_H pairs in the HG-PUL and Ara-PUL remains unknown, but is likely to increase access to additional pectins.

SGBPs contribute to glycan degradation by bringing substrates into proximity of membrane-bound enzymes⁸. Here a single SGBP encoded by each PUL was identified and shown to be specific for the target polysaccharide (Supplementary Table 5). Only SusD_Hs encoded by Gal-PUL and HG-PUL displayed affinity for their cognate glycans (Supplementary Table 5). The lack of glycan

recognition by SusD_Hs associated with the arabinan and RGI-degrading systems suggests that the corresponding SusC_H partner is required for ligand recognition. Recent structural data demonstrate that the tight association of SusC_H-D_H pairs¹⁸, supporting the concept that initial ligand recognition can require participation of both protein partners.

The oligosaccharides imported into the periplasm were degraded by GHs and PLs. The oligosaccharides generated from galactan and arabinan were depolymerized exclusively by exo-GHs, with HG and the RGI backbone by endo-PLs and exo-GHs (Supplementary Figs. 2 and 6).

With respect to galactan degradation, only a single GH2 β 1,4-galactosidase (BT4667) depolymerized galacto-oligosaccharides generated by the surface endo-galactanase (Fig. 2b and Supplementary Table 3). Surprisingly the $\Delta bt4667$ mutant displayed no growth defect on galactan (Supplementary Fig. 5). This may reflect an element of redundancy within the large number of predicted *B. thetaiotaomicron* β -galactosidases¹⁹.

Periplasmic degradation of arabinan-derived oligosaccharides was mediated by three exo- α -L-arabinofuranosidases (Supplementary Fig. 6). BT0369 removed α -1,2-L-arabinofuranose side chains²⁰. Here we demonstrate the GH51 enzymes BT0348 and BT0368 target arabinan side chains, likely to be α -1,3-arabinofuranosyl linkages, and the backbone α -1,5-arabinofuranosyl linkages, respectively (Supplementary Table 4). BT0349 released β -L-arabinose from an arabinan-derived oligosaccharide (Supplementary Fig. 7 and Supplementary Table 7). The enzyme reveals a previously unknown GH family now designated GH146 (Supplementary Fig. 8 and Supplementary Information).

RGI released from the pectin network contains remnants of arabinan, galactan and HG. Prior to RGI backbone depolymerization these accessory structures must be removed, explaining why RGI-PUL is so complex. To characterize these accessory enzymes we

used RGI from potato galactan (RGI-P), which contains many of these remnants. Galactan substitutions were cleaved from the RGI-P backbone by the synergistic action of three exo- β -1,4-galactosidases, BT4151, BT4156 and BT4160 (Supplementary Table 1). BT4160 targeted galacto-oligosaccharides, but the other two enzymes released galactose only from RGI-P. The lack of functional arabinofuranosidase genes in RGI-PUL is likely to reflect the role of single β 1,4-D-Gal units in linking arabinan chains to the RGI backbone¹³. Enzyme cocktail data indicate that BT4151 and BT4156 play a pivotal role in exposing the backbone of RGI to enzymatic attack (Supplementary Fig. 9). RGI-PUL also encodes the esterase BT4158 (Supplementary Table 1), which releases acetyl groups from D-GalA in the RGI backbone, was also shown to be important for the depolymerization of the glycan (Supplementary Fig. 9). A GH28 α -D-galacturonidase (BT4155), which targets HG (Supplementary Table 1), removed D-GalA from RGI-P but not from the glycan in *Arabidopsis mucilage* (RGI-AM), which contains no HG decorations. The crystal structure of BT4155 (Supplementary Fig. 10) revealed the expected β -helix for a GH28 enzyme²¹. In the centre of the helix is a pocket that houses three carboxylate residues that comprise the predicted catalytic apparatus based on conservation with other GH28 enzymes²² and mutagenesis data (Supplementary Table 6). The pocket extends into a channel-like structure that is likely to accommodate the conformation adopted by HG but not the RGI backbone.

In addition to enzymes classically associated with pectin degradation, RGI-PUL encodes BT4157, which is located in the apparent 'non-pectinase family' GH27. The enzyme (Supplementary Table 1) was shown to be a α -galactosidase, which is likely to target single α -galactose units that decorate the RGI backbone from Okra plants²³. Another example of enzyme diversity is the β -D-glucuronidase activity displayed by BT4181 against sugar beet arabinan in which the RGI backbone is known to contain GlcA²⁴ (Supplementary Fig. 6). It is evident, therefore, that the pectin-degrading systems are able to accommodate diversity in the fine chemistry of RGI structures from a variety of plants.

In contrast to exo-cleavage of arabinan and galactan, the backbone of RGI and HG were initially cleaved by endo-PLs and the products depolymerized by exo-GHs (Fig. 1 and Supplementary Figs. 2 and 6). The different degradative strategy is likely to reflect the high DP of the imported RGI- and HG-derived oligosaccharides compared with the neutral glycans. Thus, the initial concentration of available substrate for exo-GHs is low, but is increased by the endo-PLs. RGI-PUL encodes three periplasmic PLs. Of particular note is BT4175, which was shown to accommodate glycans appended to backbone rhamnose units (Supplementary Fig. 2), ensuring that cleavage of the (Rha-GalA)_n polymer occurred in concert with, and not subsequent to, side-chain removal.

The β -elimination of the RGI and HG backbone by the PLs generated Δ 4,5-GalA. The unsaturated residues were removed from RGI oligosaccharides with a DP of 2 or \geq 4 by BT4176 or BT4174, respectively (Supplementary Table 1); and HG oligosaccharides by BT4108 (Supplementary Table 2), which expands the activity for the GH105 family. BT4108 products were then depolymerized to GalA by the exo- α -galacturonidase BT4123 (Supplementary Table 2 and Supplementary Fig. 6). The RGI-AM oligosaccharides were degraded through the successive action of a RGI-specific GH106 α -L-rhamnosidase (BT4145) and one of three GH28 rhamnogalacturonidases (BT4146, BT4153 and BT4149) that target [D-GalAp- α -1,2-L-Rhap]_n with a DP of 2, \geq 2 or \geq 4, respectively (Supplementary Table 1). BT4145 cleaved rhamnosidic linkages through an inverting mechanism (Supplementary Fig. 11). The biological rationale for galacturonidases that target substrates with different DPs is unclear. Surprisingly deletion of BT4145 only extended the lag phase (Supplementary Fig. 5), likely to reflect the slow but complete degradation of RGI-AM by the PLs and Δ 4,5-unsaturated- α -rhamnogalacturonidases.

The ligands that activate the pectin degradative system were explored. Previously arabino-oligosaccharides with DP \geq 6 were shown to activate Ara-PUL¹⁶. Here we determined ligands that bound and activated the hybrid two-component system (HTCS) of the pectin PULs. The data (Supplementary Table 5 and Supplementary Fig. 12) demonstrate that the HTCS of Ara-PUL bound linear but not decorated arabinan, and the sensor of the Gal-PUL HTCS (BT4673) recognized small galacto-oligosaccharides. Only the oligosaccharide Δ 4,5GalA- α -1,2-Rha- α -1,4-GalA- α -1,2-Rha, a major limit product of the rhamnogalacturonan lyases, bound the HTCS (BT4178) that regulates RGI-PUL. Saturated RGI oligosaccharides failed to bind the sensor, indicating that unsaturation of the non-reducing terminal sugar is a recognition determinant. The HTCS that unregulates HG-PUL recognized only saturated HG-derived oligosaccharides. The messenger RNA levels of the *susC_H* genes of the pectin PULs showed that activation of RGI-PUL resulted in a small upregulation of HG-PUL and RGII-PUL1 (Supplementary Fig. 13). This may reflect the need to extract RGI from pectin networks through cleavage of adjacent HG segments as a prelude to its degradation.

Exo-acting enzymes that target the remnants of RGI side chains and α -1,3-L-Araf units that decorate arabinan were substantially less active than GHs that depolymerized the backbone of the respective glycans (Supplementary Tables 1 and 4). Additionally, BT4108, which removed Δ 4,5GalA from HG oligosaccharides generating the HTCS-activating ligand was slow compared with the other enzymes that act on these pectins (Supplementary Tables 1 and 2). The biological rationale for this difference in catalytic competence, may reflect the need to protect the inducing ligand (Fig. 3), as proposed for the chondroitin sulfate utilization system²⁵. Slow release of the side chain stubs or unsaturated uronic acids will block the rapid degradation of the backbone ensuring that there is continuous production of the activating molecules throughout growth on the respective glycan.

To explore pectin utilization by HGM Bacteroidetes, growth of the different species on these GalA-rich polysaccharides was determined. The data showed that only *B. ovatus*, *B. thetaiotaomicron* and *B. fingoldii* utilized all the pectins, although the majority of other organisms could grow on at least some of these glycans (Supplementary Fig. 14 and Supplementary Table 8). Around 70% of the organisms grew on HG and galactan, but only four *Bacteroides* strains utilize the RGI backbone (RGI-AM). However, 56% and 100% of the strains unable to utilize RGI-AM and potato galactan, respectively, grew on the respective oligosaccharides, demonstrating that these organisms utilize pectin degradation products. A key question is the source of oligosaccharides available to these organisms. Evidence of cross-feeding was provided by mutants of *B. thetaiotaomicron* engineered to utilize only pectic oligosaccharides (lacking the surface endo-galactanase (Δ bt4668) or RGI lyase (Δ bt4170)), which grew on the cognate polysaccharide when co-cultured with wild type *B. thetaiotaomicron* (Fig. 4a). These data show that wild-type *B. thetaiotaomicron* released polysaccharide breakdown products (PBBs; Fig. 2f) into culture media, which were available to other organisms. This is consistent with *B. uniformis* (grows on galacto-oligosaccharides but not galactan in mono-culture) utilization of the polysaccharide when co-cultured with wild-type *B. thetaiotaomicron* (Fig. 4b). This pectin cross-feeding between *B. thetaiotaomicron* and other *Bacteroides* species, however, is variable. Although *B. massiliensis* utilizes HG or RGI oligosaccharides, the bacterium failed to grow on the cognate polysaccharides when co-cultured with *B. thetaiotaomicron* (Fig. 4b). This is likely to reflect the large PBBs generated by *B. thetaiotaomicron* from these pectins, although *B. massiliensis* appears to import only RGI and HG oligosaccharides with a low DP. The lack of cross-feeding of some pectin-derived PBBs is evident in arabinan utilization. *B. ovatus* and engineered *B. thetaiotaomicron* (Δ bt0360- Δ bt0367, lacking

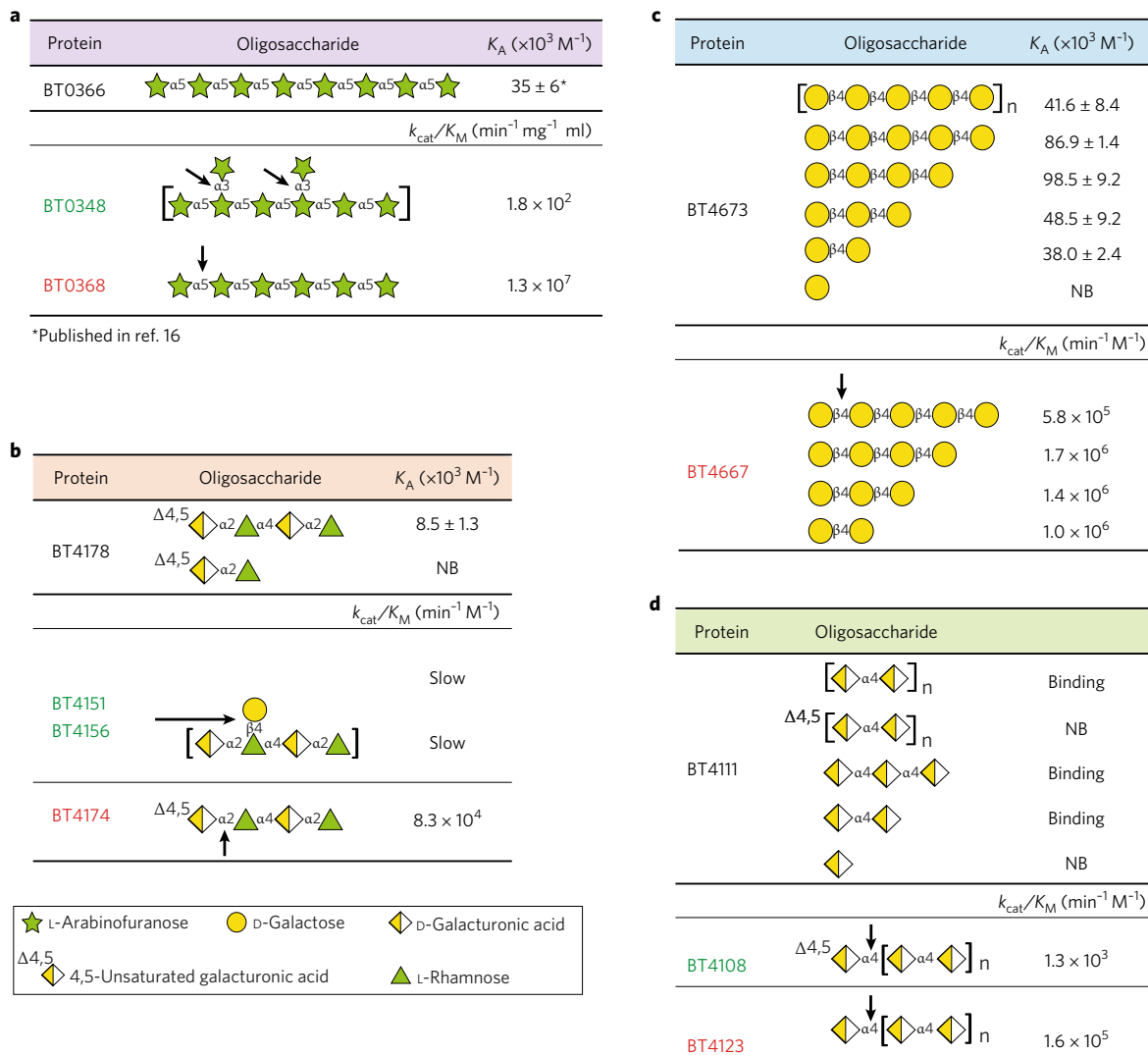


Fig. 3 | Signal molecule protection. **a–d**, Each panel shows the affinities of the signal molecules to respective sensors (top) and the catalytic efficiency of key enzymes implicated in signal molecule degradation (bottom) for galactan (**a**), arabinan (**b**), RGI (**c**) and HG (**d**). Data taken from technical replicates, $n = 3$.

the two surface endo-arabinanases) both grew on arabinooligosaccharides but not arabinan. The two organisms, however, failed to utilize arabinan when co-cultured with wild-type *B. thetaiotaomicron* (Fig. 4b). Although *B. thetaiotaomicron* released arabinooligosaccharides (Fig. 2f), the high DP of these molecules (reflects slow activity of the surface endo-arabinanases²⁰) may have prevented transport into the periplasm of these organisms.

The genetic basis of pectin utilization among the *Bacteroides* was investigated. Loci corresponding to *B. thetaiotaomicron* Gal-PUL in other *Bacteroides* species (Supplementary Fig. 15) contained an additional ORE, which, in the *B. ovatus* Gal-PUL, encodes a β -galactosidase (BACOVA_05493) with a retaining mechanism (Supplementary Fig. 16) that belongs to a previously unknown CAZy family (assigned GH147). The enzyme was particularly active against galactohexaose and galactan (Supplementary Fig. 6 and Supplementary Table 3). The importance of this enzyme is illustrated by the severe growth defect displayed by $\Delta bacova_05493$ on galactan (Fig. 2). Whole cell assays with galactan revealed the accumulation of galactose and not galacto-oligosaccharides, as occurs in *B. thetaiotaomicron*, suggesting that BACOVA_05493 is located on the bacterial surface. This was confirmed by whole cell assays of

$\Delta bacova_05493$, which revealed no products were generated from galactan. This not only demonstrates that BACOVA_05488, consistent with its very low activity (Supplementary Fig. 2), did not contribute to galactan degradation.

We examined whether the *B. thetaiotaomicron* pectin PULs provide a genetic model for *Bacteroides* utilization of these glycans. A 16S-based phylogenetic tree of the *Bacteroides* species was constructed and the organisms labelled for PUL conservation and growth on the respective oligo- and polysaccharides (Supplementary Fig. 14). There is $\geq 80\%$ agreement between the presence of a PUL and growth of the bacterium on the corresponding poly- or oligosaccharide. Growth, however, was apparent in some organisms without an equivalent PUL, showing that bacteria can deploy alternative pathways to utilize a particular glycan. There were also examples of the presence of the cognate PUL without growth of the corresponding pectin. PUL conservation was also not always congruent with the 16S phylogeny (Supplementary Fig. 14 and Supplementary Fig. 15). Thus, *B. ovatus*, *B. xylanisolvens* and *B. caccae* form a monophyletic group yet only *B. xylanisolvens* has a galactan PUL, and only *B. caccae* has lost the RGI PUL (Supplementary Fig. 14). The arabinan PUL of

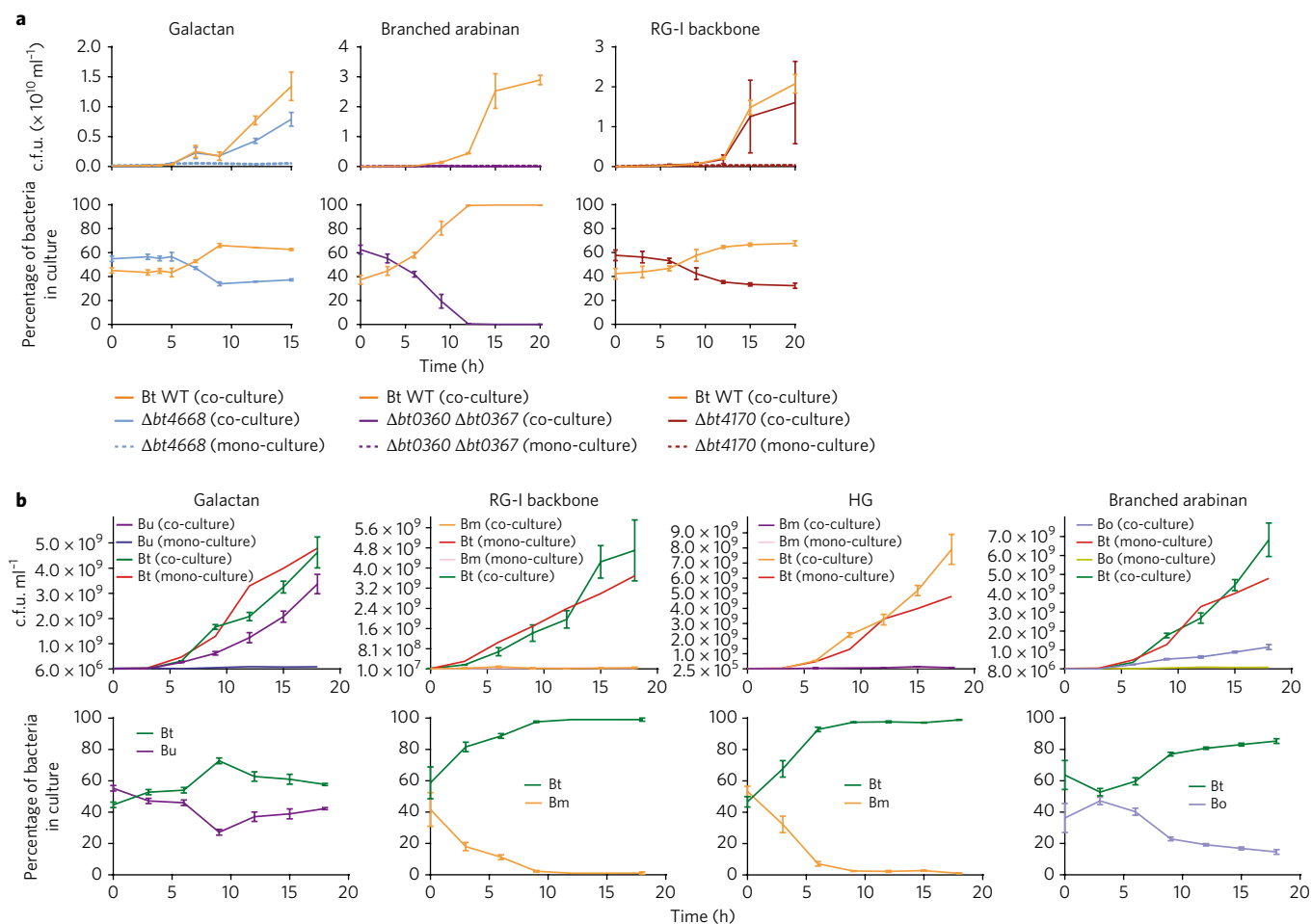


Fig. 4 | Cross-feeding of polysaccharide breakdown products between *Bacteroides* species. **a**, Wild-type *B. thetaiotaomicron* (Bt WT) and the indicated mutants of the bacterium lacking the key surface-degrading enzymes for each polysaccharide were mono-cultured and co-cultured with the wild-type bacterium as indicated. Samples were taken at different time points. The colony-forming units (c.f.u.) of these samples were determined by plating onto rich media (top panels) and the ratio of each bacterium in the culture (bottom panel) was determined by quantitative polymerase chain reaction (qPCR) with primers unique to each strain. Error bars represent the s.e.m. of biological replicates ($n=3$). **b**, *B. ovatus* (Bo), *B. massiliensis* (Bm) and *B. uniformis* (Bu) were mono-cultured or co-cultured with wild-type *B. thetaiotaomicron* (Bt) using the same experimental approach described in **a**.

B. ovatus is fragmented and that of *B. caccae* is absent (Supplementary Fig. 15a). *B. egghertii*, *B. stercoris* and *B. clarus*, also form a monophyletic group, but only *B. stercoris* has conserved the galactan PUL, and *B. egghertii* has an arabinan PUL but has lost its RGI PUL (Supplementary Fig. 15d). A final example involves *B. thetaiotaomicron* and *B. xylanisolvens*, which are closely related species, yet have different arabinan PULs. The arabinan PUL of *B. thetaiotaomicron* is identical to *B. cellulosilyticus-oleicipleus-intestinalis*, whereas the arabinan PUL of *B. xylanisolvens* is similar to *B. egghertii*. Our observations suggest that in the course of evolution *Bacteroides* rapidly gain and lose PULs that target different pectin structures.

Discussion

Combining biochemical properties and cellular location of the enzymes that target pectins with growth profiles of mutants containing gene deletions in the appropriate PULs enabled models for the metabolism of each pectic substructure, showing how the individual pathways are coordinated by *B. thetaiotaomicron* (Fig. 5). The data revealed that 30 GHs and PLs are required to degrade the major pectin domains. Given that large numbers of enzymes are also required to degrade starch and the hemicelluloses, it is evident that plant glycan metabolism explains the extremely large repertoire of CAZyme gene clusters in colonic *Bacteroides* species.

In contrast to several *Bacteroides* glycan-degrading systems where the surface GHs act slowly and target infrequent linkages^{8,26,27}, the equivalent enzymes of *B. thetaiotaomicron* that cleave galactan and the backbone of HG and RGI rapidly degrade their target polysaccharide. This is likely to reflect substrate accessibility to enzyme attack, and thus organisms with efficient surface enzymes that target accessible carbohydrates would be more competitive than bacteria in which the corresponding GHs or PLs were inefficient. This model (Fig. 5), however, does not apply to arabinan degradation where low activity of the surface enzymes was evident. This observation underpins the distinct mechanisms, distributive or selfish, by which glycans are metabolized by *Bacteroides* spp.

The RGI-PUL, in addition to orchestrating RGI backbone depolymerization, removes remnants of linked polysaccharides and single sugar sidechains (Fig. 5). In contrast, PULs that mediate degradation of other branched glycans^{8,9,26,27} depolymerize both the respective side chains and backbone structures. We propose that *B. thetaiotaomicron* does not necessarily target intact pectin structures but are able to utilize pectin domains generated by other organisms in the HGM. The RGI backbone exposed through symbiotic relationships with other intestinal microorganisms, or upstream processing by other PULs of *B. thetaiotaomicron*, is likely to contain

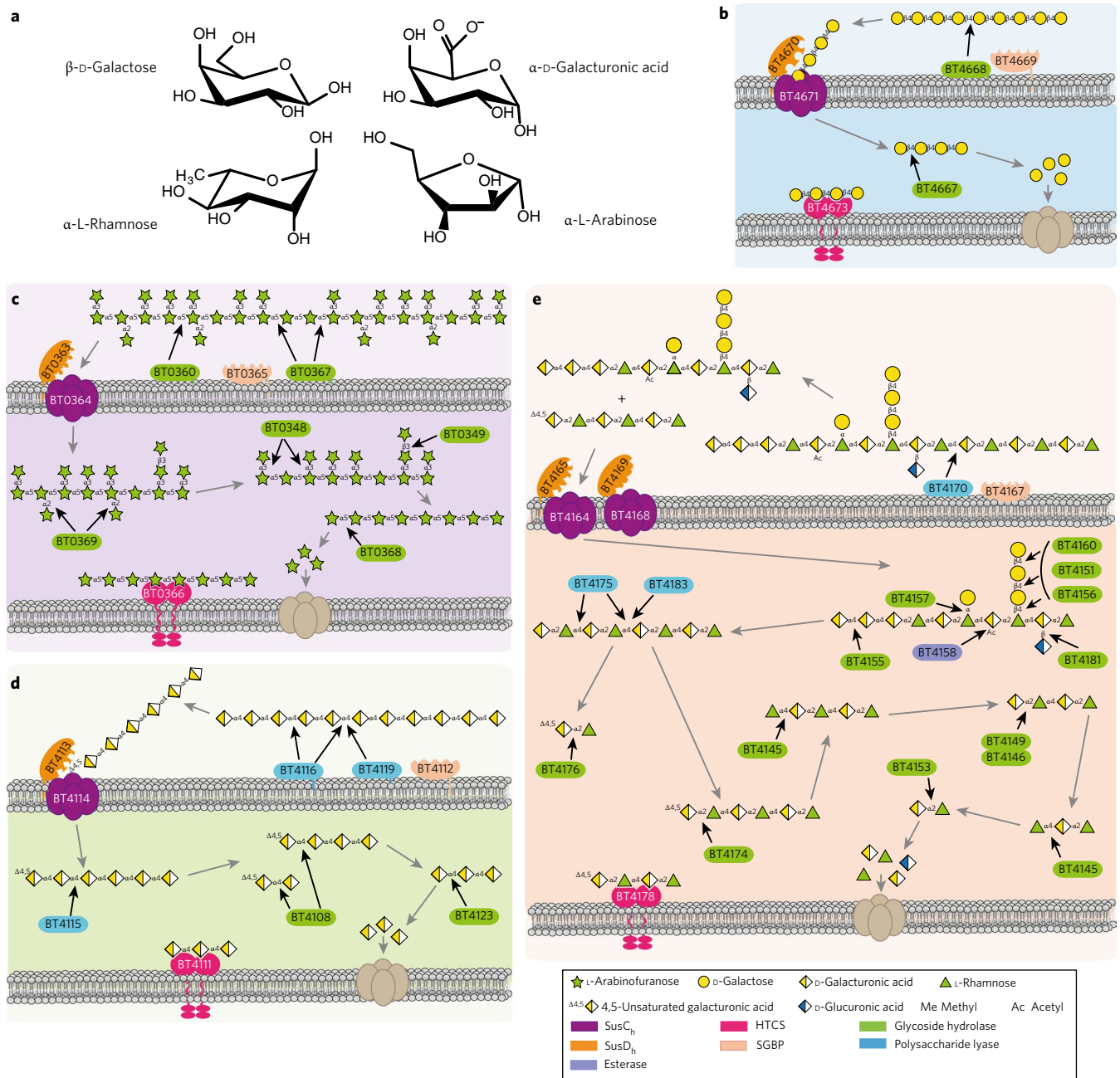


Fig. 5 | Model of pectin utilization by *B. thetaiotaomicron*. **a**, Chemical structures of the sugars in the major pectins. **b–e**, Models for degradation of galactan (**b**), arabinan (**c**), homogalacturonan (**d**) and rhamnogalacturonan I (**e**) are displayed. The black arrows indicate the linkage cleaved by the various enzymes, while the grey arrows show the direction of the degradative pathway.

additional pectin remnants explaining the complexity of enzymes encoded by the RGI-PUL.

The cross-feeding experiments demonstrate that galacto-oligosaccharides released by *B. thetaiotaomicron* are used by other organisms. The utilization of other pectin-derived PBPs, however, is more restricted. These data illustrate how glycans are made available to the general community by primary degraders. Such cross-feeding has been observed between strains of *Bacteroides* cultured on fructans and soluble starch²⁸, with the recipient organism providing a benefit to the glycan-degrading bacterium²⁹. Possible non-*Bacteroides* beneficiaries of pectin-derived cross-feeding within the HGM are *Bifidobacterium* species, which generally utilize PBPs rather than the polysaccharide²⁷. Contrasting oligosaccharide utilization profiles observed among *Bacteroides* spp. may allow co-existence of

species within the same niche targeting different components of the same glycans without competition.

The critical role played by a surface exo- β -galactosidase in galactan metabolism in some *Bacteroides* species is intriguing. This contrasts with all other *Bacteroides* glycan-degrading systems described to date, which deploy endo-acting CAZymes^{3,8,9,27,30}. These organisms may target galacto-oligosaccharides, albeit with a high DP, released by other organisms within the HGM, obviating the need for endo-cleavage. This indicates that different *Bacteroides* target galactans in distinct nutritional niches within the gut. The data also illustrate the risk associated with generating models for glycan degradation based solely on prediction of enzyme function through CAZy family assignment. To fully understand glycan metabolism a molecular genetic approach informed by biochemical

and transcriptional data in harness with bioinformatics predictions is required.

This report provides a model for how the pectic network is metabolized by a *Bacteroides* species in the HGM. Surprising variations in selective glycan metabolism and the constitution of individual pathways were apparent. This contrasts with the extensive conservation of other PULs^{9–10,27}. This suggests that organisms have adopted a variety of strategies to metabolize dietary pectins. A salient feature of pectin utilization is the elaboration of enzymes in the RGI-PUL, reflecting the requirement to remove remnants from other pectic glycans and the extraordinary number of enzymes deployed in depolymerizing the disaccharide backbone. Dissecting the mechanism of pectin degradation contributes to our understanding of the foodweb within the HGM.

Methods

Producing recombinant proteins. DNA fragments encoding predicted CAZymes and binding proteins were amplified without signal sequence by PCR using appropriate primers. The resultant DNA was then cloned into pET21a or pET28a/b linearized using appropriate restriction enzymes. The expressed protein included a His6-tag fusion at the amino (N) terminus. *Escherichia coli* strains BL21(DE3) or TUNER were transformed with the plasmids and grown to mid-exponential phase before induction with 1 mM (BL21(DE3)) or 0.2 mM (TUNER) isopropyl β -D-galactopyranoside (IPTG), and the culture was grown for a further 5 h at 37 °C or 16 h at 16 °C, respectively. The recombinant proteins were purified to >90% electrophoretic purity by immobilized metal ion affinity chromatography (IMAC) using Talon, a cobalt-based matrix, with bound proteins eluted with 100 mM imidazole, as described previously¹⁰. To generate seleno-methionine (Se-Met) proteins for structure resolution, *E. coli* cells were cultured as described previously¹⁰, and the proteins were purified using IMAC as described above. For crystallization, the Se-Met proteins were further purified by size exclusion chromatography. After IMAC, fractions containing the purified proteins were buffer-exchanged, using PD-10 Sephadex G-25M gel-filtration columns (GE Healthcare), into 10 mM Na-HEPES buffer, pH 7.5, containing 150 mM NaCl and were then subjected to gel filtration using a HiLoad 16/60 Superdex 75 column (GE Healthcare) at a flow rate of 1 ml min⁻¹. For crystallization trials, purified proteins were concentrated using an Amicon 10 kDa molecular mass centrifugal concentrator and washed three times with 5 mM dithiothreitol (for the Se-Met proteins) or water (for native proteins).

Site-directed mutagenesis. Site-directed mutagenesis was carried out employing a PCR-based NZY-Mutagenesis kit (NZYTech Ltd) using the plasmids encoding the appropriate enzymes as the template. The mutated DNA clones were sequenced to ensure that only the appropriate DNA change was introduced after the PCR.

Purification of oligosaccharides. Galacto-oligosaccharides were generated by incubation of 3 g of galactan with 100 mM HCl incubated for 3 h at 100 °C and neutralized by NaOH titration. The oligosaccharide mixture was freeze dried and resuspended in water before being applied to a P2-BioGel (BioRad) column with a 0.22 ml min⁻¹ flow rate. Fractions were evaluated for oligosaccharide content and purity by thin-layer chromatography (TLC). Pure fractions of defined oligosaccharides were pooled and concentrated. Oligosaccharide size was confirmed by mass spectrometry and high performance anion exchange chromatography (HPAEC). Crude oligosaccharide mixtures were generated by partial digestion with appropriate enzymes; BT0360 and BT0367 (arabinan), BT4668 (galactan), BT4170 (P-RGI/AM-RGI) and BT4116 (HG). Reactions were boiled and filter sterilized to remove precipitate before being evaluated by TLC.

Preparation of RGI-AM. *Arabidopsis thaliana* seeds were resuspended in distilled water (1 g ml⁻¹) and incubated at 4 °C for 16 h while stirring. The solution was centrifuged and supernatant filtered through G1 glass filter (15–40 μ m pore size). This was then dialysed against 2 \times 40 volumes of water before freeze drying. Typical yield was 1 g from 80 g of seeds.

CAZyme assays. Spectrophotometric quantitative assays for the α -L-rhamnosidase BT4145, L-arabinofuranosidases (BT0349, BT0348 and BT0368), β -D-galactosidases (BT4667, BT4151, BT4156, BT4160 and BACOVA_05493) and carbohydrate esterase (BT4158) were monitored by the formation of NADH, at $A_{340\text{nm}}$ using an extinction coefficient of 6,230 M⁻¹ cm⁻¹, with an appropriately linked enzyme assay system. The assays were adapted from purchased Megazyme International assay kits. These kits were as follows: the L-rhamnose assay kit (K-RHAMNOSE); L-arabinose–D-galactose assay kit (K-ARGA); acetic acid detection kit (K-ACET). Activity of pectic lyases (BT4170, BT4175, BT4115, BT4116) were measured at $A_{235\text{nm}}$. Activity on 4-nitrophenyl-glycosides was monitored at $A_{400\text{nm}}$. The activity of BT4668 to hydrolyse galactan was determined in 20 mM sodium phosphate buffer, pH 7.5 at 37 °C containing an appropriate

concentration of the polysaccharide and 1 mg ml⁻¹ BSA. Reactions were incubated at 37 °C and at regular time intervals 500 μ l aliquots were removed and the amount of reducing sugar was quantified using the dinitrosalicylic acid reagent²¹ and a standard curve of xylose in the reaction conditions used. Substrate depletion assays were performed as described previously⁸ to determine BT4668 activity on galacto-oligosaccharides while production of D-galactose was used to assay BT4160 activity on galactooligosaccharides. The mode of action of enzymes was determined using HPAEC or TLC, as appropriate. In brief, aliquots of the enzyme reactions were removed at regular intervals and, after boiling for 10 min to inactivate the enzyme and centrifugation at 13,000g, the amount of substrate remaining or product produced was quantified by HPAEC using standard methodology. The reaction substrates and products were bound to a Dionex CarboPac PA100 (galactooligosaccharides–arabino-oligosaccharides), PA1 (monosaccharides) or PA20 (polygalacturonic acid oligosaccharides) column and glycans eluted with an initial isocratic flow of 100 mM NaOH then a 0–200 mM sodium acetate gradient in 100 mM NaOH at a flow rate of 1.0 ml min⁻¹, using pulsed amperometric detection. Linked assays were checked to make sure that the relevant enzyme being analysed was rate limiting by increasing its concentration and ensuring a corresponding increase in rate was observed. A single substrate concentration was used to calculate catalytic efficiency (k_{cat}/K_M), and was checked to be markedly less than K_M by halving and doubling the substrate concentration and observing an appropriate increase or decrease in rate. The equation $V_0 = (k_{\text{cat}}/K_M)[S][E]$ was used to calculate k_{cat}/K_M unless substrate depletion was used then the calculation was as follows $\ln(k_{\text{cat}}/K_M) = (S_0/S_t)/[E]$, in which $[E]$ and $[S]$ are enzyme and substrate concentration, respectively. All reactions were carried out in 20 mM sodium phosphate buffer, pH 7.0, with 150 mM NaCl (defined as standard conditions) and performed in at least technical triplicates.

Isothermal titration calorimetry. The binding of proteins to their glycan ligands was quantified by isothermal titration calorimetry, as described previously²⁷. Titrations were carried out in 50 mM Na-HEPES buffer, pH 7.5 at 25 °C. The reaction cell contained protein at 50–100 μ M, and the syringe contained either the oligosaccharide at 1–10 mM or the polysaccharide at 3–10 mg ml⁻¹. Integrated heats were fitted to a single-site model using Microcal Origin v7.0 to derive n , K_D , and ΔH values. ΔG and ΔS were calculated from the equation $-R\ln K_D = \Delta G = \Delta H - T\Delta S$ where R is the gas constant and T is the temperature in Kelvins.

Electrospray ionization mass spectrometry. The molecular mass of purified oligosaccharides (in 10 mM ammonium acetate, pH 7.0) was analysed via negative ion mode infusion–offline electrospray ionization mass spectrometry following dilution (typically 1:1 (v/v)) with 5% trimethylamine in acetonitrile.

Electrospray data were acquired using a linear trap quadrupole-Fourier transform mass spectrometer (Thermo) with a resolution setting of 100,000 at $m/z = 400$ and an injection target value of 1,000,000. Infusion spray analyses were performed on 5–10 μ l of samples using medium ‘nanoES’ spray capillaries (Thermo) for offline nanospray mass spectrometry in negative ion mode at 1 kV.

¹H-NMR determination of catalytic mechanism. Enzymes BT4145 and BACOVA_05493 were freeze dried in 20 mM Tris-HCl, 500 mM NaCl, pH 7.5 as were substrates α -L-Rha- α 1,4-D-GalA and (β 1,4-Galp)₃, respectively and resuspended in deuterium oxide. Prior to addition of enzyme an initial ¹H-NMR spectra was obtained. Enzyme was added and spectra recorded at appropriate time intervals. The ratio of α - and β -monosaccharide products was determined to deduce catalytic mechanism.

2D NMR of arabinotetraose before and after treatment with BT0349. NMR spectra were recorded at 298 K in D₂O with a Bruker AVANCE III spectrometer operating at 600 MHz equipped with a TCI CryoProbe. Two-dimensional ¹H–¹H total correlation spectroscopy (TOCSY), rotating frame nuclear Overhauser spectroscopy (ROESY), double quantum filtered correlation spectroscopy (DQFCOSY), ¹³C heteronuclear single quantum coherence (HSQC) and HSQC-TOCSY experiments were performed, using established methods³²; the mixing times were 70 ms and 200 ms for the TOCSY and ROESY experiments, respectively. Chemical shifts were measured relative to internal acetone ($\delta_{\text{H}} = 2.225$, $\delta_{\text{C}} = 31.07$ ppm). Data were processed using the Azara suite of programs (v. 2.8, copyright 1993–2017, Wayne Boucher and Department of Biochemistry, University of Cambridge, unpublished) and chemical-shift assignment was performed using Analysis v2.4³³.

Growth of *Bacteroides* and generation of mutants. *Bacteroides* mutants were generated by deletion or replacement of the target gene with an inactive version by counter selectable allelic exchange using the pExchange-tdk plasmid. The full method is described in ref. ³⁴. Mutants generated in this study are distinguished by the locus tag of the gene deleted/inactivated ($\Delta btxxx$ or $\Delta bacovaxxxxx$).

Bacteroides spp. were routinely cultured under anaerobic conditions at 37 °C using an anaerobic cabinet (Whitley A35 Workstation; Don Whitley) in culture volumes of 0.2, 2 or 5 ml) of TYG (tryptone–yeast extract–glucose medium) or minimal medium (MM) containing 0.5–1% of an appropriate carbon source and 1.2 mg ml⁻¹ porcine haematin (Sigma-Aldrich) as previously described⁹.

The growth of the cultures was routinely monitored at $A_{600\text{nm}}$ using a Biochrom WPA cell density meter for the 5 ml cultures or a Gen5 v2.0 Microplate Reader (Biotek) for the 0.2 and 2 ml cultures.

Protein cellular localization. Cellular localization of proteins was carried out as described previously⁸. In brief, *B. thetaiotaomicron* cultures were grown overnight ($A_{600\text{nm}}$ value of 2.0) in 5 ml MM containing 0.5% potato rhamnolacturonan I (P-RGI) or homogalacturonan. The next day, cells were collected by centrifugation at 5,000g for 10 min and resuspended in 2 ml of PBS. Proteinase K (0.5 mg ml⁻¹ final concentration) was added to 1 ml of the suspension and the other half left untreated (control). Both samples were incubated at 37°C overnight followed by centrifugation (5,000g for 10 min) to collect cells. To eliminate residual proteinase K activity, cell pellets were resuspended in 1 ml of 1.5 M trichloroacetic acid and incubated on ice for 30 min. Precipitated mixtures were then centrifuged (5,000g, 10 min) and washed twice in 1 ml of ice-cold acetone (99.8%). The resulting pellets were allowed to dry in a 40°C heat block for 5 min and dissolved in 250 µl of Laemmli buffer. Samples were heated for 5 min at 98°C and mixed by pipetting several times before resolving by SDS-PAGE using 12% gels. Electrophoresed proteins were transferred to nitrocellulose membranes by Western blotting followed by immunochemical detection using primary rabbit polyclonal antibodies (Eurogentec) generated against various proteins and secondary goat anti-rabbit antibodies (Santa Cruz Biotechnology). For BT4119 the anti-sera failed to produce the desired reactivity. Thus, a carboxy (C)-terminal Flag peptide (DYKDDDDK) was incorporated at the C-terminals of the native proteins expressed by *B. thetaiotaomicron* through counter-selectable allelic exchange³⁴. This allowed their detection using rabbit anti-Flag antibodies (Sigma) as primary antibodies. In the case of BT4668, BT0360 and BT0367 mutations (that lead to the inactivation of the encoded enzymes) were made in each gene within the *B. thetaiotaomicron* genome to generate the mutants $\Delta bt4668$, $\Delta bt0360$, $\Delta bt0367$ and $\Delta bt0360/\Delta bt0367$. Cells were grown in MM containing 0.5% arabinose- or galacto-oligosaccharides to activate the target PULs. The cells were harvested from mid-log phase 5 ml cultures and concentrated in 0.5 ml of PBS. The resuspended cells were incubated with the target glycans in an aerobic environment, conditions in which only the activity of the surface enzymes can be monitored. At appropriate time intervals samples were taken and subjected to HPAEC analysis. The data were compared with that of wild-type *B. thetaiotaomicron* to explore whether the loss in enzyme activity occurred at the bacterial surface.

Cross-feeding and competition assays. Prior to co-culture each *Bacteroides* sp. was grown in TYG and washed in PBS before being used to inoculate MM containing 0.5% glycan. Samples of 0.5 ml were taken at regular intervals during growth, which were serially diluted and plated onto Brain-Heart Infusion (BHI, Sigma-Aldrich) with agar and porcine haematin for determination of the total CFU per ml of the culture. Genomic DNA was purified from the remainder of the sample (Bacterial genomic DNA purification kit, Sigma-Aldrich). Quantitative PCR was used to determine the ratio of different *Bacteroides* spp. or mutants in the sample using primers specific for unique regions in each *Bacteroides* sp. genome or tag introduced into one of two *att* sites. The ratio of each species/mutant was used to calculate the CFU per ml of each organism in the culture.

Quantitative RT-PCR (RT-qPCR). Comparison of the levels of transcription of *susC* homologues (*susC_H*) from each of the pectin PULs was performed by RT-qPCR. Previous studies have shown *susC_H* genes are a good proxy for expression of their cognate PUL³⁵. *B. ovatus* was cultured in 5 ml of MM containing 0.5% (w/v) carbon source, as described above. Triplicate bacterial cultures were harvested at mid-log phase (A_{600} ~0.8) and placed in RNAlater (Qiagen), then stored at -80°C overnight, before purification with RNeasy kit (Qiagen). RNA purity was assessed spectrophotometrically, and 1 µg of RNA was used immediately for reverse transcription (QuantiTect Reverse Transcription kit, Qiagen). RT-qPCR was performed in a 96-well plate on a LightCycler 480 System (Roche) with FastStart Essential DNA Green Master (Roche) using the standard primer. Reactions were carried out in 10 µl, consisting of 5 µl of SYBR Green mix, 20 ng of complementary DNA and 1 µM (*susC_H* genes) or 0.125 µM (16S ribosomal RNA) primer mix. Reaction conditions were 95°C for 600 s, followed by 45 cycles of 95°C for 10 s, 55°C for 10 s, 72°C for 10 s. Cq values (cycle at which an amplification signal is first detected) were calculated using a LightCycler 480 SW 1.5. Data were normalized to 16S rRNA transcript levels, and a change in expression level was calculated as a fold change compared with minimal media, glucose cultures.

Crystal structure determination. *Crystallization.* All proteins were concentrated to 10 mg ml⁻¹. BT4170 native crystallized in 20 mM sodium/potassium phosphate 20% (w/v) polyethylene glycol (PEG) 3350. BT4170 co-crystallized with 10 mM of oligosaccharide reaction products generated by BT4170 (defined as ligand) in 100 mM succinic acid, sodium phosphate glycine buffer at pH 6.0 and 25% (w/v) PEG 1500. BT4170 inactive mutant K285A was co-crystallized with 30 mM ligand in 200 mM potassium chloride and 20% PEG 3350. Selenomethionine-containing BT4155 crystallized in 200 mM sodium chloride, 100 mM Bis-Tris buffer pH 5.5 and 25% PEG 3350. BT0349 with 500 mM L-arabinose was crystallized in 20% PEG 3350 and 200 mM ammonium formate. All samples were cryo-protected by supplementing the mother liquor with 20% PEG 400.

Data collection and processing. BT0349, BT4170 and BT4170 K285A ligand data were indexed and integrated with the automated pipeline Xia2 (3da protocol)³⁶. BT4170 in complex with ligand and BT4155 were indexed and integrated with XDS³⁷. The data were scaled with either XDS or Aimless³⁸. Space group determination was confirmed with Pointless³⁹. The phase problem for BT0349 and BT4155 was solved by SeMet-SAD using hkl2map⁴⁰ and the shelx pipeline⁴¹. BT4170 native apo data were solved by molecular replacement with the pipeline Balbes⁴² with the PDB model 1RU4 as search model. Initial models of BT0349, BT4155 and BT4170 were improved by successive runs of automated model building program arp_warp⁴³ and buccaneer⁴⁴. BT4170 TRI SCACCHARIDE and BT4170 inactive mutant K285A data were solved using the 4170 native apo model. All models were refined and improved using successive cycle of Refmac⁴⁵ and manual model building with Coot⁴⁶. All models were validated using Coot⁴⁶ and molprobit⁴⁷. Five per cent of the observations were randomly selected for the Rfree set. The data processing, refinement statistics and Protein Data Bank (PDB) codes are reported in Supplementary Table 9.

Comparative genomics analysis. PULs similar to the RGI, galactan, arabinan and homogalacturonan PULs were searched in HGM Bacteroidetes genomes. The identification of similar PULs was based on PUL alignments. Gene composition and order of Bacteroidetes PULs were computed using the PUL predictor described in PULDB⁴⁸. Then, in a manner similar to amino acid sequence alignments, the predicted PULs were aligned to the appropriate pectin PULs according to their modularity as proposed in the RADS/RAMPAGE method⁴⁹. Modules taken into account include CAZy families, sensor-regulators and *suscd*-like genes. Finally, PUL boundaries and limit cases were refined by BLASTP-based analysis. The previously unknown glycoside hydrolase families discovered in this study are listed in the main text.

Life Science Reporting Summary. Further information on experimental design is available in the Life Sciences Reporting Summary.

Data availability. The data that support the findings of this study are available from the corresponding author upon request. The authors declare that the data supporting the findings of this study are available within the paper and the Supplementary Information. Complete western blot images are provided in Supplementary Fig. 1. The crystal structure datasets generated (coordinate files and structure factors) have been deposited in the PDB and are listed in Supplementary Table 9 together with the PDB accession codes.

Received: 21 September 2017; Accepted: 20 November 2017;
Published online: 18 December 2017

References

- Caffall, K. H. & Mohnen, D. The structure, function, and biosynthesis of plant cell wall pectic polysaccharides. *Carbohydr. Res.* **344**, 1879–1900 (2009).
- Gilbert, J. A. et al. Microbiome-wide association studies link dynamic microbial consortia to disease. *Nature* **535**, 94–103 (2016).
- Sonnenburg, J. L. & Backhed, F. Diet-microbiota interactions as moderators of human metabolism. *Nature* **535**, 56–64 (2016).
- Koropatkin, N. M., Cameron, E. A. & Martens, E. C. How glycan metabolism shapes the human gut microbiota. *Nat. Rev. Microbiol.* **10**, 323–335 (2012).
- Desai, M. S. et al. A dietary fiber-deprived gut microbiota degrades the colonic mucus barrier and enhances pathogen susceptibility. *Cell* **167**, 1339–1353 (2016).
- Wu, M. et al. Genetic determinants of in vivo fitness and diet responsiveness in multiple human gut Bacteroides. *Science* **350**, aac5992 (2015).
- Cartmell, A. et al. How members of the human gut microbiota overcome the sulfation problem posed by glycosaminoglycans. *Proc. Natl Acad. Sci. USA* **114**, 7037–7042 (2017).
- Cuskin, F. et al. Human gut Bacteroidetes can utilize yeast mannans through a selfish mechanism. *Nature* **517**, 165–169 (2015).
- Larsbrink, J. et al. A discrete genetic locus confers xyloglucan metabolism in select human gut Bacteroidetes. *Nature* **506**, 498–502 (2014).
- Ndeh, D. et al. Complex pectin metabolism by gut bacteria reveals novel catalytic functions. *Nature* **544**, 65–70 (2017).
- Lombard, V., Golaconda Ramulu, H., Drula, E., Coutinho, P. M. & Henrissat, B. The carbohydrate-active enzymes database (CAZy) in 2013. *Nucleic Acids Res.* **42**, 490–495 (2014).
- Gilbert, H. J. The biochemistry and structural biology of plant cell wall deconstruction. *Plant Physiol.* **153**, 444–455 (2010).
- Lau, J. M., Mcneil, M., Darvill, A. G. & Albersheim, P. Treatment of rhamnolacturonan-I with lithium in ethylenediamine. *Carbohydr. Res.* **168**, 245–274 (1987).
- Coenen, G. J., Bakx, E. J., Verhoef, R. P., Schols, H. A. & Voragen, A. G. J. Identification of the connecting linkage between homo- or xylogalacturonan and rhamnolacturonan type I. *Carbohydr. Polym.* **70**, 224–235 (2007).
- Bonnin, E., Garnier, C. & Ralet, M. C. Pectin-modifying enzymes and pectin-derived materials: applications and impacts. *App. Microbiol. Biotechnol.* **98**, 519–532 (2014).

16. Martens, E. C. et al. Recognition and degradation of plant cell wall polysaccharides by two human gut symbionts. *PLoS Biol.* **9**, e1001221 (2011).
17. Martens, E. C., Koropatkin, N. M., Smith, T. J. & Gordon, J. I. Complex glycan catabolism by the human gut microbiota: the Bacteroidetes Sus-like paradigm. *J. Biol. Chem.* **284**, 24673–24677 (2009).
18. Glenwright, A. J. et al. Structural basis for nutrient acquisition by dominant members of the human gut microbiota. *Nature* **541**, 407–411 (2017).
19. Xu, J. et al. A genomic view of the human-*Bacteroides thetaiotaomicron* symbiosis. *Science* **299**, 2074–2076 (2003).
20. Cartmell, A. et al. The structure and function of an arabinan-specific α -1,2-arabinofuranosidase identified from screening the activities of bacterial GH43 glycoside hydrolases. *J. Biol. Chem.* **286**, 15483–15495 (2011).
21. Pickersgill, R., Smith, D., Worboys, K. & Jenkins, J. Crystal structure of polygalacturonase from *Erwinia carotovora* ssp. *carotovora*. *J. Biol. Chem.* **273**, 24660–24664 (1998).
22. van Santen, Y. et al. 1.68-angstrom crystal structure of endopolygalacturonase II from *Aspergillus niger* and identification of active site residues by site-directed mutagenesis. *J. Biol. Chem.* **274**, 30474–30480 (1999).
23. Sengkhampan, N. et al. Okra pectin contains an unusual substitution of its rhamnosyl residues with acetyl and alpha-linked galactosyl groups. *Carbohydr. Res.* **344**, 1842–1851 (2009).
24. Renard, C. M., Crepeau, M. J. & Thibault, J. F. Glucuronic acid directly linked to galacturonic acid in the rhamnogalacturonan backbone of beet pectins. *Eur. J. Biochem.* **266**, 566–574 (1999).
25. Raghavan, V., Lowe, E. C., Townsend, G. E. 2nd, Bolam, D. N. & Groisman, E. A. Tuning transcription of nutrient utilization genes to catabolic rate promotes growth in a gut bacterium. *Mol. Microbiol.* **93**, 1010–1025 (2014).
26. Bagenholm, V. et al. Galactomannan catabolism conferred by a polysaccharide utilization locus of *Bacteroides ovatus*: enzyme synergy and crystal structure of a beta-mannanase. *J. Biol. Chem.* **292**, 229–243 (2017).
27. Rogowski, A. et al. Glycan complexity dictates microbial resource allocation in the large intestine. *Nat. Commun.* **6**, 7481 (2015).
28. Rakoff-Nahoum, S., Coyne, M. J. & Comstock, L. E. An ecological network of polysaccharide utilization among human intestinal symbionts. *Curr. Biol.* **24**, 40–49 (2014).
29. Rakoff-Nahoum, S., Foster, K. R. & Comstock, L. E. The evolution of cooperation within the gut microbiota. *Nature* **533**, 255–259 (2016).
30. Foley, M. H., Cockburn, D. W. & Koropatkin, N. M. The Sus operon: a model system for starch uptake by the human gut Bacteroidetes. *Cell Mol. Life Sci.* **73**, 2603–2617 (2016).
31. Miller, G. L. Use of dinitrosalicylic acid reagent for determination of reducing sugar. *Anal. Chem.* **31**, 426–428 (1959).
32. Cavanagh, J., Fairbrother, W. J., Palmer, A. G. & Skelton, N. J. *Protein NMR Spectroscopy: Principles and Practice* (Academic Press, Cambridge, 1996).
33. Vranken, W. F. et al. The CCPN data model for NMR spectroscopy: development of a software pipeline. *Proteins* **59**, 687–696 (2005).
34. Koropatkin, N. M., Martens, E. C., Gordon, J. I. & Smith, T. J. Starch catabolism by a prominent human gut symbiont is directed by the recognition of amylose helices. *Structure* **16**, 1105–1115 (2008).
35. Despres, J. et al. Unraveling the pectinolytic function of *Bacteroides xylanisolvens* using a RNA-seq approach and mutagenesis. *BMC Genomics* **17**, 147 (2016).
36. Winter, G. xia2: an expert system for macromolecular crystallography data reduction. *J. Appl. Crystallogr.* **43**, 186–190 (2010).
37. Kabsch, W. XDS. *Acta Crystallogr. D* **66**, 125–132 (2010).
38. Evans, P. R. & Murshudov, G. N. How good are my data and what is the resolution? *Acta Crystallogr. D* **69**, 1204–1214 (2013).
39. Evans, P. R. An introduction to data reduction: space-group determination, scaling and intensity statistics. *Acta Crystallogr. D* **67**, 282–292 (2011).
40. Pape, T. & Schneider, T. R. HKL2MAP: a graphical user interface for macromolecular phasing with SHELX programs. *J. Appl. Crystallogr.* **37**, 843–844 (2004).
41. Sheldrick, G. M. Experimental phasing with SHELXC/D/E: combining chain tracing with density modification. *Acta Crystallogr. D* **66**, 479–485 (2010).
42. Long, F., Vagin, A. A., Young, P. & Murshudov, G. N. BALBES: a molecular-replacement pipeline. *Acta Crystallogr. D* **64**, 125–132 (2008).
43. Langer, G., Cohen, S. X., Lamzin, V. S. & Perrakis, A. Automated macromolecular model building for X-ray crystallography using ARP/wARP version 7. *Nat. Protoc.* **3**, 1171–1179 (2008).
44. Cowtan, K. Fitting molecular fragments into electron density. *Acta Crystallogr. D* **64**, 83–89 (2008).
45. Vagin, A. A. et al. REFMAC5 dictionary: organization of prior chemical knowledge and guidelines for its use. *Acta Crystallogr. D* **60**, 2184–2195 (2004).
46. Emsley, P. & Cowtan, K. Coot: model-building tools for molecular graphics. *Acta Crystallogr. D* **60**, 2126–2132 (2004).
47. Chen, V. B. et al. MolProbity: all-atom structure validation for macromolecular crystallography. *Acta Crystallogr. D* **66**, 12–21 (2010).
48. Terrapon, N., Lombard, V., Gilbert, H. J. & Henrissat, B. Automatic prediction of polysaccharide utilization loci in Bacteroidetes species. *Bioinformatics* **31**, 647–655 (2015).
49. Terrapon, N., Weiner, J., Grath, S., Moore, A. D. & Bornberg-Bauer, E. Rapid similarity search of proteins using alignments of domain arrangements. *Bioinformatics* **30**, 274–281 (2014).
50. Varki, A. et al. Symbol nomenclature for graphical representations of glycans. *Glycobiology* **25**, 1323–1324 (2015).

Acknowledgements

This work was supported in part by an Advanced Grant from the European Research Council (Grant No. 322820) awarded to H.J.G. and B.H. supporting A.S.L., D.N., A.C. and N.T., a Wellcome Trust Senior Investigator Award to H.J.G. (grant No. WT097907MA) that supported J.B. and E.C.L. a European Union Seventh Framework Initial Training Network Programme entitled the “WallTraC project” (Grant Agreement number 263916) awarded to M.-C.R. and H.J.G, which supported X.Z. and J.S. The Biotechnology and Biological Research Council project ‘Ricefuel’ (grant numbers BB/K020358/1) awarded to H.J.G. supported A.L. We thank Diamond Light Source for access to beamline I02, I04-1 and I24 (mx1960, mx7854 and mx9948) that contributed to the results presented here, and to J. Gray at Newcastle University for assistance with the mass spectrometry.

Author contributions

Enzyme characterization was carried out by A.S.L., J.B., X.Z., A.L., I.V., R.M., K.Sh, B.F. and J.S. The generation of oligosaccharide products was carried out by M.-C.R., X.Z., A.S.L., A.C. and D.N. Gene deletion strains were constructed by A.S.L., D.N., R.M., B.F., J.B. and D.W.A. Co-culturing experiments were carried out by J.B. and A.S.L. Phylogenetic reconstruction and metagenomic analysis was by N.T. and B.H. Bacterial growth and transcriptomic experiments were by X.Z., E.C.L. and E.C.M. X-ray protein crystallography was by A.B., A.C., A.S.L. and J.B. NMR experiments were by A.S.L. and K.St. Experiments were designed by D.W.A., H.J.G., E.C.L., S.C.M. and H.J.G. The manuscript was written by H.J.G. with substantial contributions from D.W.A., E.C.L., N.T. and B.H. Figures were prepared by E.C.L. and A.S.L.

Competing interests

The authors declare no competing financial interests.

Additional information

Supplementary information is available for this paper at <https://doi.org/10.1038/s41564-017-0079-1>.

Reprints and permissions information is available at www.nature.com/reprints.

Correspondence and requests for materials should be addressed to D.W.A. or H.J.G.

Publisher's note: Springer Nature remains neutral with regard to jurisdictional claims in published maps and institutional affiliations.

Life Sciences Reporting Summary

Nature Research wishes to improve the reproducibility of the work that we publish. This form is intended for publication with all accepted life science papers and provides structure for consistency and transparency in reporting. Every life science submission will use this form; some list items might not apply to an individual manuscript, but all fields must be completed for clarity.

For further information on the points included in this form, see Reporting Life Sciences Research. For further information on Nature Research policies, including our data availability policy, see Authors & Referees and the Editorial Policy Checklist.

▶ Experimental design

1. Sample size

Describe how sample size was determined.

All the enzyme kinetic data in Supplementary Tables 1, 2, 3, 4 and 6 and isothermal titration calorimetry binding data in Supplementary Tables 5 represent a minimum of technical triplicates. The data for a few of the enzymes were biological triplicates. The microbial experiments reported in Table 8, Fig. 2a and Supplementary Fig. 5 represent 3 biological replicates with each replicate repeated twice. The bars in the qRT-PCR experiment in Supplementary Figure 13 represent 6 biological replicates with the values for the individual experiments shown. Analysis of microbial products in Fig. 2b and Supplementary Figures 2, 4, 6, 7 and 9 were a minimum of biological duplicates. The examples of NMR data in Supplementary Figures 11 and 16 are examples of biological duplicates. Localization experiments using antibodies in Fig. 2c and Supplementary Figure 1 are examples of biological triplicates. Where shown errors were standard errors of the mean.

2. Data exclusions

Describe any data exclusions.

No data were excluded from the analysis.

3. Replication

Describe whether the experimental findings were reliably reproduced.

All attempts at replication were successful.

4. Randomization

Describe how samples/organisms/participants were allocated into experimental groups.

The randomization was not relevant in this study where only in intro assay were performed.

5. Blinding

Describe whether the investigators were blinded to group allocation during data collection and/or analysis.

The blinding was not relevant in this study where only in intro assay were performed.

Note: all studies involving animals and/or human research participants must disclose whether blinding and randomization were used.

6. Statistical parameters

For all figures and tables that use statistical methods, confirm that the following items are present in relevant figure legends (or in the Methods section if additional space is needed).

n/a Confirmed

- The exact sample size (n) for each experimental group/condition, given as a discrete number and unit of measurement (animals, litters, cultures, etc.)
- A description of how samples were collected, noting whether measurements were taken from distinct samples or whether the same sample was measured repeatedly
- A statement indicating how many times each experiment was replicated
- The statistical test(s) used and whether they are one- or two-sided (note: only common tests should be described solely by name; more complex techniques should be described in the Methods section)
- A description of any assumptions or corrections, such as an adjustment for multiple comparisons
- The test results (e.g. P values) given as exact values whenever possible and with confidence intervals noted
- A clear description of statistics including central tendency (e.g. median, mean) and variation (e.g. standard deviation, interquartile range)
- Clearly defined error bars

See the web collection on statistics for biologists for further resources and guidance.

► Software

Policy information about availability of computer code

7. Software

Describe the software used to analyze the data in this study.

Growth curves and Real time-qPCR data were analyzed using Prism Graphpad software or Gen5 software (BioTek). Microcal Origin v7.0 was used to analyze Isothermal Titration Calorimetry data. NMR data was analyzed with Azara suite of programs (v. 2.8, copyright 1993-2017, Wayne Boucher and Department of Biochemistry, University of Cambridge, unpublished) and chemical shift assignment was performed using CCPNMR Analysis v2.4.

For manuscripts utilizing custom algorithms or software that are central to the paper but not yet described in the published literature, software must be made available to editors and reviewers upon request. We strongly encourage code deposition in a community repository (e.g. GitHub). *Nature Methods* guidance for providing algorithms and software for publication provides further information on this topic.

► Materials and reagents

Policy information about availability of materials

8. Materials availability

Indicate whether there are restrictions on availability of unique materials or if these materials are only available for distribution by a for-profit company.

All unique materials used are readily available from the authors or from standard commercial sources.

9. Antibodies

Describe the antibodies used and how they were validated for use in the system under study (i.e. assay and species).

Protein cell localization was performed by immunochemical detection using primary rabbit polyclonal antibodies (Eurogentec) generated against various proteins and secondary goat anti-rabbit antibodies (sc-2004, Santa Cruz Biotechnology). Primary rabbit polyclonal antibodies specificity was validated by the specific immunochemical detection of purified protein. FLAG-Tagged proteins were detected using rabbit anti-Flag antibodies (F7425, Sigma).

10. Eukaryotic cell lines

a. State the source of each eukaryotic cell line used.

No eukaryotic cell lines were used.

b. Describe the method of cell line authentication used.

No eukaryotic cell lines were used.

c. Report whether the cell lines were tested for mycoplasma contamination.

No eukaryotic cell lines were used.

d. If any of the cell lines used are listed in the database of commonly misidentified cell lines maintained by ICLAC, provide a scientific rationale for their use.

No eukaryotic cell lines were used.

► Animals and human research participants

Policy information about studies involving animals; when reporting animal research, follow the ARRIVE guidelines

11. Description of research animals

Provide details on animals and/or animal-derived materials used in the study.

No animals were used.

Policy information about studies involving human research participants

12. Description of human research participants

Describe the covariate-relevant population characteristics of the human research participants.

The study did not involve human research participants.